Why liquids can appear to solidify during squeeze-out – even when they don't

Hongyu Gao*, Martin H. Müser

Dept. of Materials Science and Engineering, Universität des Saarlandes, 66123 Saarbrücken, Germany

Abstract

When liquids are squeezed out between two solid surfaces, they often exhibit layering, load-bearing ability, and a much increased viscosity. The combination of these phenomena is frequently interpreted as confinement-induced solidification. Here we propose that such behavior may often better be rationalized as the non-zero wavevector response of a pressurized liquid: bulk liquids contain structure even beyond the nanoscale as evidenced by their (damped) sinusoidal density correlations. Under confinement, this structure enables liquids to sustain non-isotropic stresses and thereby to carry load over a time span that is long enough for molecules to rearrange in the confined zone. In response to the load, viscosity can increase locally, in which case liquid flow is suppressed. This interpretation is supported by molecular-dynamics simulations of a key commercial base-oil component (1-decene trimer), which is squeezed out between a ridge and a substrate. The layering of the oil reflects the density correlations of the bulk liquid. At the same time, the confined liquid can sustain von Mises stresses exceeding locally 100 MPa over sufficiently long times for molecules to diffuse within the confined zone.

Keywords: liquids, confinement, tribology, molecular-dynamics

*Corresponding author
Email addresses: hongyu.gao@uni-saarland.de (Hongyu Gao), martin.mueser@mx.uni-saarland.de (Martin H. Müser)

1. Introduction

When liquids are confined to a narrow gap between a tip and a substrate, their properties often appear to change dramatically with respect to the bulk, most notably layering [1, 2] and a much enhanced effective shear viscosity [3, 4, 5]. The observed phenomena can arise due to a confinement-induced transition of the liquid into a crystal [6, 7] or into a disordered solid [8], while in some cases, unexpected behavior of liquids may also simply be the consequence of artifacts. Examples for the latter can either arise from residual nanoparticles on solid surfaces [9] or be due to the use of commensurate, confining walls, which enable even a gaseous interlayer to mediate a static friction force between two (sufficiently large) non-interacting surfaces [10].

While perturbations, such as confining walls, may certainly induce phase transformations when a liquid is close to a liquid-solid or liquid-glass transformation [11, 12, 13], layering and load-bearing ability are observed quite commonly. One problem with using 'confinement-induced solidification' as the sole explanation for the observed phenomena is that signs of thermodynamic anomalies can be missing even when systems appear to solidify otherwise [14]. In addition, simulations of alkanes confined at ambient pressure to a thin slit reveal that their viscosity has similar temperature and shear-rate dependences as in the bulk [15]. Last but not least, the load-bearing ability of many liquids increases rather continuously with a decreasing number of layers [1] rather than in ways indicative of a phase or a glass transition. In fact, the *layer-by-layer* squeeze-out process of liquids as disjunct as an ionic liquid [16] and hexane [5], can be described with free-energy expressions [5] reflecting the functional form of ordinarily found bulk-liquid density autocorrelation functions (ACF) [17, 18, 19]. The underlying picture within a continuum, i.e., density-functional theory based description of liquids [18, 19] would be that layering and thus load-bearing ability arise naturally from the liquid's wavenumber dependent compressibility, because the one-particle density of a confined liquid has a similar functional form as the two-particle density of a bulk liquid. In other words, the heterogeneity of liq-

uids at small scales allows them to possess a non-isotropic stress tensor under confinement [20], thereby giving them the ability to sustain shear and load for reasons unrelated to surface tension. In contrast, anisotropy, be it induced by confining walls [21] or due to molecular ordering in liquid crystals, is not sufficient to make a liquid load bearing, because flow still occurs in response to an anisotropic stress.

Several interesting questions arise, which have been scarcely investigated. How anisotropic is the stress tensor of a load-bearing liquid? What is the maximum possible deviatoric stress that a liquid can sustain on time scales clearly exceeding cage lifetime or structural relaxation time? If anisotropic stress is retained after molecules have rearranged in the gap, the liquid would be in (slow) flow and yet not yield. This is an interesting state of matter, since the conventional definition of a fluid (and thus of its subcategory liquid) is its ability to conform to the shape of the container holding it, which can be cast as a fluid's inability to sustain non-isotropic bulk stresses over extended times. Last but not least, what factor(s) control the molecular mobility in the confined zone and thereby the resistance to sliding?

To address this set of questions, we use molecular-dynamics (MD) to simulate the squeeze-out process of an important component of commercial base oils, namely 1-decene trimer, which is sandwiched between a blunt ridge and a flat substrate. We chose this branched molecule because it has less propensity to order than a linear alkane. The blunt ridge was preferred over a curved tip for mainly two reasons: First, using a constant-height indenter removes the necessity of having to interpret the result as a superposition of the laws valid for flat indenters. Second, the sample volume for a ridge is greater than for a curved tip with the added benefit of improving statistics while increasing the free-energy barrier for the elimination of monolayers.

2. Model and Methods

Our model system consists of a base oil (1-decene trimer, $C_{30}H_{62}$) either in the bulk or sandwiched between confining walls, which reflect Fe(100) surfaces. In the latter case, both walls are atomically flat (locally). However, one wall is an indenter with a rectangular ridge at its bottom. The substrate and the bottom layer of the ridge are strongly adhesive, while the other indenter walls are repulsive. The set-up is similar to a previously used one, which allowed the lubricant to be squeezed into a reservoir at an essentially constant chemical potential [22]. A cross-section of the default set-up including the structure of 1-decene trimer is shown in Fig. 1. Details on the model and the set-up are given next.

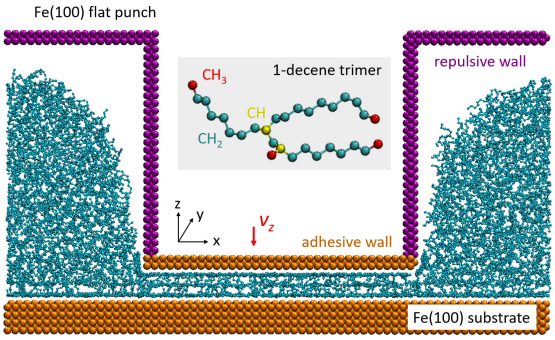

Figure 1: Snapshot of the default system. Orange "iron" (Fe) atoms make an adhesive interaction with the lubricant, while purple iron atoms interact solely with repulsion. The spacing between the indenter's bottom layer and the substrate's top layer is $d = 1.48$ nm in this image. The molecular structure of an individual base oil molecule (1-decene trimer) is shown as well.

Interactions. The interactions within the liquid systems were described with a united-atom model [23], in which monomers, i.e., CH_3, CH_2, and CH, were treated as point masses. The intra-molecular potential contains harmonic energy expressions for bond stretching, bending as well as a term penalizing torsion. Interactions between non-bonded united atoms were modeled with a 12-6 Lennard-

Jones (LJ) potentials using the Lorentz-Berthelot (LB) mixing rules [24, 25]. The employed force-field parameters were taken from Refs. [26, 27, 28, 29] and are provided in the S.I. They were successfully used in the past, for example, to describe the slip-boundary conditions of confined n-alkanes [30] or their shear thinning [31].

Interactions between iron and united atoms were again modeled with 12-6 LJ potential by applying the LB mixing rules. The LJ parameters for iron were taken from Ref. [29]. For flat walls, a cutoff radius of 2.5 σ was employed, leading to a relatively strong adsorption of the branched alkanes. Interactions between united atoms and iron atoms in the repulsive parts of the ridge were cut off at $\sqrt[6]{2}\ \sigma$ so that the molecules adsorbed preferentially to the substrate and to the bottom of the indenter. The goal was not necessarily to have a realistic model for alkanes with iron – or iron atoms would have had to be passivated with oxygen – but to produce boundary conditions for the fluid so as to match macroscopic observations. In that sense, our simulations pertain to (smooth) solid surfaces in general that attracting alkanes strongly enough to prevent interfacial slippage, although changes in chemical detail can certainly alter the morphology of adsorbed molecules and thereby their slip-boundary condition [32] or squeeze-out process [33].

Geometry and dimensions. The geometry of the default system is shown in Fig. 1 with a distance of $d = 1.48$ nm between the bottom tip layer and the top substrate layer. The dimensions of the cell along x and y directions are 20.0×5.1 in units of nm. The distance between the bottom layer of the indenter and the top layer of the substrate is varied in the range of 0.7 nm $< d <$ 3.0 nm. The height of the ridge is $h = 8.6$ nm. $N_{\mathrm{m}} = 450$ molecules were included in the default system resulting in a homogeneous, approximately six-layer thick liquid film adsorbed onto the substrate in the absence of a counter surface. The ridge started to be in contact with the liquid at a separation of $d = 4.0$ nm.

Wall atoms in both the tip and the substrate were fixed relative to their assigned center-of-mass velocity of the respective solid throughout. These constraints did not vary results in a significant fashion compared to results obtained

in initial test runs, in which the topmost substrate atoms were unconstrained and their interactions modeled with the embedded-atom method (EAM) potential [34]. The purpose here was to lower the computational cost as much as we can. All liquid atoms were free to propagate according to Newton's equation of motion. Periodic boundary conditions were applied in the xy-plane; while, in the z-direction, atoms were restricted to move by the solid walls.

In order to validate force-field parameters and acquire bulk liquid properties, additional simulations were conducted based on a pure bulk liquid system with periodic boundary conditions applied in all three dimensions. In this case, $N_{\mathrm{m}} = 200$ molecules were modeled in a cubic cell with an equilibrium cell volume of 183.2 nm^3 at ambient pressure for a duration of 2 ns relaxation and 3 ns observation.

Operating conditions. In the default configuration, the substrate was kept in place and the tip pushed down at constant velocities ranging from $v_z = 0.2$ m/s to $v_z = 5.0$ m/s. In some cases, the tip was stopped and the system relaxed at a given separation d. All squeeze-out simulations were conducted at $T = 300$ K, maintained by a Langevin thermostat with a damping time of 100 fs. In these cases, the thermostat was only applied to the y-component of the velocities so as to minimize the possible affects on the sliding forces. The simulation time-step was 1 fs.

Observables. A central property deduced from our simulations is the mean stress averaged over a central volume V_{c} between the indenter and the substrate. The stress-tensor components were computed only when compression was halted and the system relaxed at constant wall-wall separations. For the calculation of the stress, we used the virial estimator, which is only rigorous for homogeneous systems in thermal equilibrium [35, 21]. (Due to the presence of bending and torsional terms in the potential energy surface, we were not aware of more accurate ways to rigorously define stress locally, such as the "stress/mop" method implemented in LAMMPS [36].) The central volume V_{c} extended over $l_{x,\mathrm{c}}$ being the central 80% along the x-direction between the punch and the substrate, the full length along the periodically y-direction, and the confined gap d in z-

direction. The virial theorem based estimation for σ_{zz} was fairly constant below the full area of the punch and quickly dropped to zero outside of it. Its precise value was chosen such that the (relaxed) stress tensor element σ_{zz} was on par with the externally imposed force (on the ridge) divided by the total area of the ridge. Stress tensor components obtained this way were always rather close to those obtained by integrating the virial estimator over the distance between two relative density minima. This is why we are confident that the results of the stress tensor components are sufficiently reliable to draw the conclusions herein this work and that errors on the von Mises stress (defined and discussed in the following paragraph) should not exceed $O(10\%)$.

The von Mises stress σ_{vM} is defined through the equation

$$\sigma_{\mathrm{vM}}^2 \equiv \left\{(\sigma_1^{\mathrm{p}} - \sigma_2^{\mathrm{p}})^2 + (\sigma_2^{\mathrm{p}} - \sigma_3^{\mathrm{p}})^2 + (\sigma_3^{\mathrm{p}} - \sigma_1^{\mathrm{p}})^2\right\}/2$$

where the $\sigma_\alpha^{\mathrm{p}}$ with $\alpha = 1, ..., 3$ denote the principal values or eigenvalues of the stress tensor. The von Mises stress is the most commonly used measure for predicting plastic flow of solids in the context of continuum mechanics. Plastic flow is expected to occur when σ_{vM} exceeds a material-specific threshold value. To obtain σ_{vM} in our simulations, all stress-tensor elements were first computed in bins of size $0.5\ \mathrm{nm} \times l_y \times 0.5\ \mathrm{nm}$, of which those in the central confined region were averaged. Here, $l_y = 5.1$ nm is the system size in the periodically repeated direction parallel to the ridge.

Used code. All MD simulations were performed using the open-source code LAMMPS [36].

3. Results

The goal of this work is to enhance our understanding of the phenomena that accompany the squeeze-out process of fluids. As such, we are not interested in a highly accurate reproduction of the squeeze-out process in a specific contact. The used model merely needs to reproduce trends reasonably well, which it certainly achieves for the base-oil under consideration: at ambient conditions,

the bulk liquid density turned out to be $\rho = 0.783$ g/cm^3, in good agreement with the experimentally-measured value of $\rho = 0.780$ g/cm^3 [37]. The modeled compressibility was $\kappa = 1.12$ GPa^{-1}, for which we could not identify an experimental reference number. However, our value is close to $\kappa = 0.83$ GPa^{-1}, which was found experimentally for an isomeric poly-alpha-olefin [38]. The temperature-dependent viscosity as well as the shear-thinning behavior of the used model also compared reasonably well to experimental data or other computational studies [39, 31]. These claims are substantiated in the S.I.

The first central result of this work is that the period of the density oscillations in the bulk liquid (liq), $\lambda_{\rm liq} = 4.63$ Å, closely matches the distance between density maxima in the confined liquid (cfd), i.e., $\lambda_{\rm cfd} = 4.50$ Å. The values for the two wavelengths were obtained from a fit to the radial distribution function $g(r)$ in the liquid as described in Eq. (1) and from a fit to $\rho(z)$ in the confined plane-parallel wall geometry as described in Eq. (2). In detail, the deviations of $g(r)$ from unity are known to obey

$$r\{g(r) - 1\} \propto \sin\left(\frac{2\pi\, r}{\lambda_{\rm cfd}} + \varphi\right)\, e^{-r/\zeta} \tag{1}$$

in three dimensions for large values of r, where ζ is a correlation length and φ a dimensionless phase. Note that we show r-times the expression on the l.h.s. of Eq. (1) in Fig. 2(a), in order to reveal more clearly the decay of the oscillations in $g(r)$ at large r. For the case of two plane-parallel walls, the fit to density oscillations, as shown in Fig. 2(b), was based on the symmetrized function

$$\begin{aligned} \rho(z) - \rho_0 \quad \propto \quad & e^{-(z+d/2)/\zeta} \cos\left\{\frac{2\pi}{\lambda_{\rm cfd}}\left(z + \frac{d}{2}\right) + \varphi\right\} \\ & + e^{+(z-d/2)/\zeta} \cos\left\{\frac{2\pi}{\lambda_{\rm cfd}}\left(z - \frac{d}{2}\right) - \varphi\right\}, \end{aligned} \tag{2}$$

which reflects the expected density correlations for a large wall-wall separation d in an effective one-dimensional geometry, in which $z = 0$ lies half way between the two confining walls. Moreover, ρ_0 is the bulk fluid density.

The values for $\lambda_{\rm liq}$ and $\lambda_{\rm cfd}$ are not only close to each but they are also close to the separation between two force maxima, which is $\Delta d \approx 0.42$ nm as

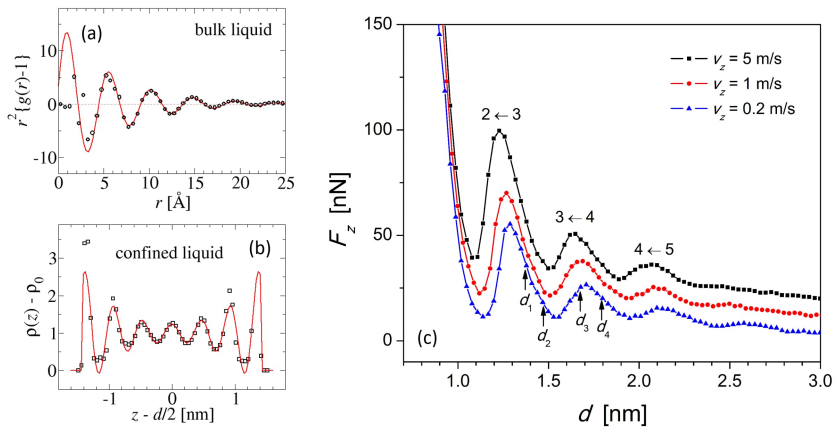

Figure 2: Representation of density oscillations in (a) the bulk liquid and (b) confined geometry. Symbols show simulation results, while lines reflect fits of the data to Eqs. (1) and (2), respectively. (c) Force $F(d)$ as a function of wall-wall separation d at three different velocities. The force maxima occur when the number of confined layers starts to reduce from $(n+1) \to n$, as marked by arrows. Selected distances, to which references are made in the text, are also marked by arrows.

shown in Fig. 2(c) and as obtained during compression with constant velocity. Thus, not only the *functional form* of the bulk-liquid density-ACF correlates with undulations of force maxima—as already revealed previously, for example, for a short linear alkane [5] and an ionic liquid [16]—but also the *numerical values* for the periods. This close correlation between bulk liquid and confined liquid properties is surprising in the light of a relatively large confinement, in which the wall-wall separation d has fallen clearly below the radius of gyration of molecules in bulk liquid of $R_g \approx 0.57$ nm.

The heterogeneity of liquids at small scales implies their abilities to sustain non-isotropic stresses under confinement. We next investigate to what extent the stress tensor does remain anisotropic after relaxation at a given wall-wall separation d. Towards this end, configurations occuring during the $v = 0.2$ m/s compression run are saved at selected values of d and later used for follow-up runs at fixed wall-wall separation. As expected, the stress tensor is anisotropic,

as shown exemplarily in Fig. 3(a) for $d_3 = 1.68$ nm. In fact, the von Mises stress turns out to be 520, 74, 139, and 31 MPa at d_1, d_2, d_3, and d_4, respectively. Some of these values are quite large i.e., even at the relatively large separation d_3, it is close to the macroscopic yield strength of aluminum.

(a) (b)

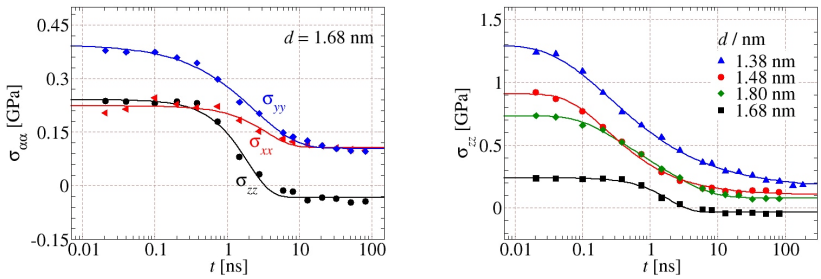

Figure 3: Relaxation of stress tensor elements, $\sigma_{\alpha\alpha}$, as a function of time t and as deduced from the virial estimator averaged over a 48.6 nm^3 large central volume between the punch and the substrate. During the relaxation, the seperation between the confining walls remains fixed at the specified values of d. (a) σ_{xx}, σ_{yy}, σ_{zz} at the separation $d = 1.68$ nm. (b) σ_{zz} at different values of d.

The existence of a long plateau in all stress tensor components with non-identical principal values, which was observed for any given value of d, implies that the liquid has relaxed to thermal equilibrium, or, has reached at least metastability. The question arises to what degree molecules in the confined liquid remain mobile while sustaining a non-isotropic stress. To address this question, the in-plane mean-square displacement (MSD) was measured by averaging over all monomers from molecules whose center-of-mass was initially part of the central volume defined above. Monomers in the layers adjacent to a wall were excluded from the measurement. Averaging started only after the stress-tensor elements had closely approached their final plateau values, e.g., after $t_0 = 100$ ns for $d = 1.38$ nm and after $t_0 = 30$ ns for $d = 1.68$ and 1.48 nm.

For all studied separations, the motion of the monomers remains sub-diffusive in a time span of 200 ns. However, even at the highest confinement of $d_1 =$

1.38 nm, monomers displaced averagely over 4 Å during this time span. Such a distance itself may certainly be considered small. However, it clearly exceeds the expected distances of atoms displacing in a crystalline structure when the generation of a dislocation releases von Mises stresses exceeding the yield strength of a crystal. In contrast, in our case, no notable stress relaxation took place over the time span of $O(100\,\mathrm{ns})$ after t_0. This does not only hold for the normal but for all stress tensor components. Thus, the results indicate that the studied fluid is able to sustain non-isotropic stresses, while being in a (plastic) flow. This observation further confirms previous simulations, in which liquids composed of short linear alkanes were found to be in the full diffusive regime while being load-bearing [40].

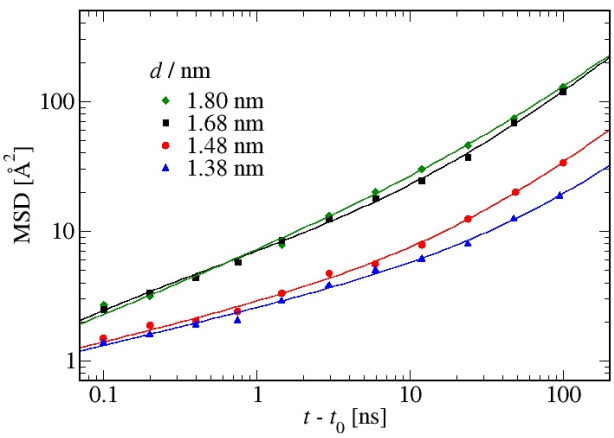

Figure 4: Mean-square displacement of molecules originally located in the central volume, after stress relaxation.

Last but not least, Fig. 4 reveals that the mobility of the polymers does not decrease monotonically with increasing confinement. At $d_4 = 1.80$ nm, monomers appear to have diffused roughly the same distance as those under a larger confinement of $d_3 = 1.68$ nm during the first 200 ns and appear even less

mobile when extrapolating the data to times $t \gtrsim 200$ ns. Surprisingly, such a behavior has scarcely, if ever, been discussed. It can be rationalized by the observation that the normal stress is greater at d_4 than at d_3, see Fig. 3(b), whereby (laminar) flow at d_4 is more strongly impeded. For the two additional investigated cases, i.e., $d_2 = 1.48$ nm and $d_1 = 1.38$ nm, both the normal pressure and confinement are larger than those at $d_{3,4}$, which lead to even lower mobility. The decrease in mobility is relatively moderate with confinement and pressure, which is an indication of the absence of any long-range or even intermediate-range ordering of the confined molecules. To demonstrate the absence of long-range order, a representative view of the in-plane molecular arrangement is shown in Fig. 5.

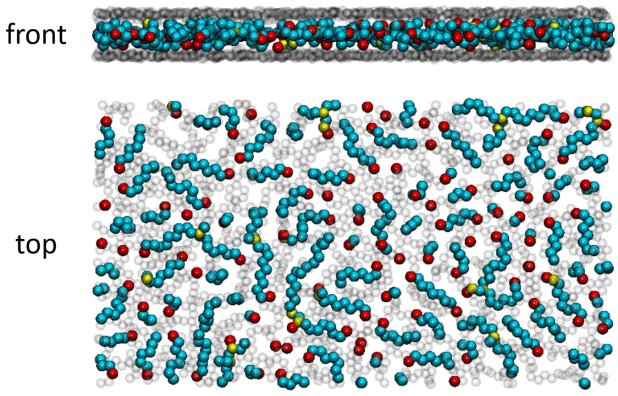

Figure 5: A representative view of monomers in the center layer of the confined film for a piston-substrate separation of $d = 1.38$ nm after 200 ns equilibration.

4. Discussion and Conclusions

Our study revealed that branched lubricants (e.g. 1-decene trimer) under confinement, while remaining in the liquid state, can sustain non-isotropic stresses and thereby being load-bearing. The presence of non-isotropic stresses is certainly not surprising by itself. However, the value of a von Mises stress

on the order of 100 MPa in the case of a triple-layer boundary film is close to the order of the macroscopic yield stress of various metals (e.g. aluminum). Given how much a single-layer graphene placed on top of stepped or amorphous metal surfaces increases their plastic yield [41], our results might complement the picture of how lubricants protect solid surfaces. The confined liquids do not only prevent metal surfaces from massive intimate contact, they also mitigate peak von Mises stresses in the solids, which they protect, or even move the von Mises stress maxima from the solids into the lubricant.

A previous study on the squeeze-out of linear alkanes correlated the enhanced load-bearing ability to the existence of 2D solid-like states when the molecules are longer chains [42]. Similarly, a large resistance to squeeze-out may also be related to ordering in non-polymeric systems, such as simple model systems of ionic liquids [43], which furthermore allow the effect of surface-liquid to be studied by simple voltage manipulation. While we believe the correlation between molecular ordering and load-bearing ability does exist for the just-mentioned systems, our study on branched polymers clearly revealed that quasi-static load-bearing ability requires neither crystallization nor a glass transition to occur.

The necessity of system-specific answers certainly extends from the load-bearing ability to other properties such as the change of kinetic or static friction on load or confinement. For our system, we find indications that the mobility of the molecules is not a monotomic function of the confinement, but that the normal stress can matter as well, i.e., the mobility of molecules can increase (against an overall trend) with increasing confinement when the normal pressure has decreased after the expulsion of a monolayer. While oils generally increase their viscosity roughly exponentially with (hydrostatic) pressure, water does not [44, 45] and instead may even become more fluidic.

To conclude, we wish to comment on Steve Granick's assessment in his pioneering study on motions and relaxation of confined liquids [4]: *The flow of liquids under extreme confinement cannot be understood simply by intuitive extrapolation of bulk properties.* This statement is certainly true if bulk properties are meant to be bulk properties in the long wavelength limit. However, bulk flu-

ids have wave-vector dependent compressibility, giving rise to density oscillations in the liquid, which very much resemble the density oscillations in confinement. This brings up the interesting question to what degree other properties (such as the von Mises stress of a confined liquid at a given chemical potential and wall-wall separation) can be rationalized or perhaps even predicted quantitatively from field theories for complex fluids [46] using bulk liquid properties in addition to confining walls alone. Regarding such an extrapolation from bulk liquids to confined liquids, we side with Steve Granick and believe this work requires more than simple intuition.

[1] R. G. Horn, J. N. Israelachvili, Direct measurement of structural forces between two surfaces in a nonpolar liquid, The Journal of Chemical Physics 75 (3) (1981) 1400–1411. doi:10.1063/1.442146.
URL https://doi.org/10.1063/1.442146

[2] H. Christenson, R. Horn, J. Israelachvili, Measurement of forces due to structure in hydrocarbon liquids, Journal of Colloid and Interface Science 88 (1) (1982) 79–88. doi:10.1016/0021-9797(82)90156-4.
URL https://doi.org/10.1016/0021-9797(82)90156-4

[3] J. V. Alsten, S. Granick, Molecular tribometry of ultrathin liquid films, Physical Review Letters 61 (22) (1988) 2570–2573. doi:10.1103/physrevlett.61.2570.
URL https://doi.org/10.1103/physrevlett.61.2570

[4] S. Granick, Motions and relaxations of confined liquids, Science 253 (5026) (1991) 1374–1379. doi:10.1126/science.253.5026.1374.
URL https://doi.org/10.1126/science.253.5026.1374

[5] M.-D. Krass, N. N. Gosvami, R. W. Carpick, M. H. Müser, R. Bennewitz, Dynamic shear force microscopy of viscosity in nanometer-confined hexadecane layers, Journal of Physics: Condensed Matter 28 (13) (2016) 134004. doi:10.1088/0953-8984/28/13/134004.
URL https://doi.org/10.1088/0953-8984/28/13/134004

[6] P. A. Thompson, M. O. Robbins, Origin of stick-slip motion in boundary lubrication, Science 250 (4982) (1990) 792–794. doi:10.1126/science.250.4982.792.
URL https://doi.org/10.1126/science.250.4982.792

[7] P. A. Thompson, G. S. Grest, M. O. Robbins, Phase transitions and universal dynamics in confined films, Physical Review Letters 68 (23) (1992) 3448–3451. doi:10.1103/physrevlett.68.3448.
URL https://doi.org/10.1103/physrevlett.68.3448

[8] J. Klein, E. Kumacheva, Confinement-induced phase transitions in simple liquids, Science 269 (5225) (1995) 816–819. doi:10.1126/science.269.5225.816.
URL https://doi.org/10.1126/science.269.5225.816

[9] M. Heuberger, M. Zäch, Nanofluidics: structural forces, density anomalies, and the pivotal role of nanoparticles, Langmuir 19 (6) (2003) 1943–1947. doi:10.1021/la026645p.
URL https://doi.org/10.1021/la026645p

[10] M. H. Müser, M. O. Robbins, Conditions for static friction between flat crystalline surfaces, Physical Review B 61 (3) (2000) 2335–2342. doi:10.1103/physrevb.61.2335.
URL https://doi.org/10.1103/physrevb.61.2335

[11] C. L. Jackson, G. B. McKenna, Vitrification and crystallization of organic liquids confined to nanoscale pores, Chemistry of Materials 8 (8) (1996) 2128–2137. doi:10.1021/cm9601188.
URL https://doi.org/10.1021/cm9601188

[12] S. T. Cui, P. T. Cummings, H. D. Cochran, Molecular simulation of the transition from liquidlike to solidlike behavior in complex fluids confined to nanoscale gaps, The Journal of Chemical Physics 114 (16) (2001) 7189–7195. doi:10.1063/1.1359736.
URL https://doi.org/10.1063/1.1359736

[13] C. Alba-Simionesco, B. Coasne, G. Dosseh, G. Dudziak, K. E. Gubbins, R. Radhakrishnan, M. Sliwinska-Bartkowiak, Effects of confinement on freezing and melting, Journal of Physics: Condensed Matter 18 (6) (2006) R15–R68. doi:10.1088/0953-8984/18/6/r01.
URL https://doi.org/10.1088/0953-8984/18/6/r01

[14] D. F. Kienle, T. L. Kuhl, Density and phase state of a confined nonpolar fluid, Physical Review Letters 117 (3). doi:10.1103/physrevlett.117.036101.
URL https://doi.org/10.1103/physrevlett.117.036101

[15] I. M. Sivebaek, V. N. Samoilov, B. N. J. Persson, Effective viscosity of confined hydrocarbons, Physical Review Letters 108 (3). doi:10.1103/physrevlett.108.036102.
URL https://doi.org/10.1103/physrevlett.108.036102

[16] J. Hoth, F. Hausen, M. H. Müser, R. Bennewitz, Force microscopy of layering and friction in an ionic liquid, Journal of Physics: Condensed Matter 26 (28) (2014) 284110. doi:10.1088/0953-8984/26/28/284110.
URL https://doi.org/10.1088/0953-8984/26/28/284110

[17] M. E. Fisher, B. Wiodm, Decay of correlations in linear systems, The Journal of Chemical Physics 50 (9) (1969) 3756–3772. doi:10.1063/1.1671624.
URL https://doi.org/10.1063/1.1671624

[18] K. Nygård, S. Sarman, K. Hyltegren, S. Chodankar, E. Perret, J. Buitenhuis, J. F. van der Veen, R. Kjellander, Density fluctuations of hard-sphere fluids in narrow confinement, Physical Review X 6 (1). doi:10.1103/physrevx.6.011014.
URL https://doi.org/10.1103/physrevx.6.011014

[19] K. Nygård, Local structure and density fluctuations in confined fluids, Current Opinion in Colloid & Interface Science 22 (2016) 30–34. doi:

10.1016/j.cocis.2016.02.005.
URL https://doi.org/10.1016/j.cocis.2016.02.005

[20] J.-C. Wang, K. A. Fichthorn, A method for molecular dynamics simulation of confined fluids, The Journal of Chemical Physics 112 (19) (2000) 8252–8259. doi:10.1063/1.481430.
URL https://doi.org/10.1063/1.481430

[21] R. Hartkamp, A. Ghosh, T. Weinhart, S. Luding, A study of the anisotropy of stress in a fluid confined in a nanochannel, The Journal of Chemical Physics 137 (4) (2012) 044711. arXiv:https://doi.org/10.1063/1.4737927, doi:10.1063/1.4737927.
URL https://doi.org/10.1063/1.4737927

[22] Y. Wang, K. Hill, J. G. Harris, Confined thin films of a linear and branched octane. a comparison of the structure and solvation forces using molecular dynamics simulations, The Journal of Chemical Physics 100 (4) (1994) 3276–3285. doi:10.1063/1.466418.
URL https://doi.org/10.1063/1.466418

[23] S. O. Nielsen, C. F. Lopez, G. Srinivas, M. L. Klein, Coarse grain models and the computer simulation of soft materials, Journal of Physics: Condensed Matter 16 (15) (2004) R481–R512. doi:10.1088/0953-8984/16/15/r03.
URL https://doi.org/10.1088%2F0953-8984%2F16%2F15%2Fr03

[24] H. A. Lorentz, Ueber die anwendung des satzes vom virial in der kinetischen theorie der gase, Ann. Phys. 248 (1881) 127–136.

[25] D. Berthelot, Sur le melange des gaz, Comptes. Rendus. Acad. Sci. 126 (1898) 1703–1855.

[26] W. L. Jorgensen, J. Tirado-Rives, The opls [optimized potentials for liquid simulations] potential functions for proteins, energy minimizations for

crystals of cyclic peptides and crambin, J. Am. Chem. Soc. 110 (1988) 1657–1666.

[27] W. D. Cornell, P. Cieplak, C. I. Bayly, I. R. Gould, K. M. Merz, D. M. Ferguson, D. C. Spellmeyer, T. Fox, J. W. Caldwell, P. A. Kollman, A second generation force field for the simulation of proteins, nucleic acids, and organic molecules, J. Am. Chem. Soc. 117 (1995) 5179–5197.

[28] L. Zhang, R. Balasundaram, S. H. Gehrke, S. Jiang, Nonequilibrium molecular dynamics simulations of confined fluids in contact with the bulk, J. Chem. Phys. 114 (2001) 6869–6877.

[29] H. Berro, N. Fillot, P. Vergne, Molecular dynamics simulation of surface energy and zddp effects on friction in nano-scale lubricated contacts, Tribol. Int. 43 (2010) 1811–1822.

[30] D. Savio, N. Fillot, P. Vergne, M. Zaccheddu, A model for wall slip prediction of confined n-alkanes: Effect of wall-fluid interaction versus fluid resistance, Tribol. Lett. 46 (2012) 11–22.

[31] P. Liu, J. Lu, H. Yu, N. Ren, F. E. Lockwood, Q. J. Wang, Lubricant shear thinning behavior correlated with variation of radius of gyration via molecular dynamics simulations, J. Chem. Phys. 147 (2017) 084904.

[32] L.-T. Kong, C. Denniston, M. H. Müser, The crucial role of chemical detail for slip-boundary conditions: molecular dynamics simulations of linear oligomers between sliding aluminum surfaces, Modelling and Simulation in Materials Science and Engineering 18 (3) (2010) 034004. doi: 10.1088/0965-0393/18/3/034004.
URL https://doi.org/10.1088%2F0965-0393%2F18%2F3%2F034004

[33] M.-D. Krass, G. Krämer, U. Dellwo, R. Bennewitz, Molecular layering in nanometer-confined lubricants, Tribology Letters 66 (3) (2018) 87. doi: 10.1007/s11249-018-1041-y.
URL https://doi.org/10.1007/s11249-018-1041-y

[34] M. Mendelev, S. Han, D. Srolovitz, G. Ackland, D. Sun, M. Asta, Development of new interatomic potentials appropriate for crystalline and liquid iron, Philos. Mag. 83 (2003) 3977–3994.

[35] B. D. Todd, D. J. Evans, P. J. Daivis, Pressure tensor for inhomogeneous fluids, Phys. Rev. E 52 (1995) 1627–1638. doi:10.1103/PhysRevE.52.1627.
URL https://link.aps.org/doi/10.1103/PhysRevE.52.1627

[36] S. Plimpton, Fast parallel algorithms for short-range molecular dynamics, J. Comput. Phys. 117 (1995) 1–19.

[37] T. Zolper, Z. Li, C. Chen, M. Jungk, T. Marks, Y.-W. Chung, Q. Wang, Lubrication properties of polyalphaolefin and polysiloxane lubricants: Molecular structure–tribology relationships, Tribology Letters 48 (3) (2012) 355–365. doi:10.1007/s11249-012-0030-9.
URL https://doi.org/10.1007/s11249-012-0030-9

[38] H. E. Grandelli, J. S. Dickmann, M. T. Devlin, J. C. Hassler, E. Kiran, Volumetric properties and internal pressure of poly(-olefin) base oils, Industrial & Engineering Chemistry Research 52 (50) (2013) 17725–17734. arXiv:https://doi.org/10.1021/ie402644w, doi:10.1021/ie402644w.
URL https://doi.org/10.1021/ie402644w

[39] P. Liu, H. Yu, N. Ren, F. E. Lockwood, Q. J. Wang, Pressure–viscosity coefficient of hydrocarbon base oil through molecular dynamics simulations, Tribology Letters 60 (3) (2015) 34. doi:10.1007/s11249-015-0610-6.
URL https://doi.org/10.1007/s11249-015-0610-6

[40] R.-G. Xu, Y. Xiang, Y. Leng, Computational simulations of solvation force and squeezing out of dodecane chain molecules in an atomic force microscope, The Journal of Chemical Physics 147 (5) (2017) 054705. arXiv:https://doi.org/10.1063/1.4996886, doi:10.1063/1.4996886.
URL https://doi.org/10.1063/1.4996886

[41] A. Klemenz, A. Gola, M. Moseler, L. Pastewka, Contact mechanics of graphene-covered metal surfaces, Applied Physics Letters 112 (6) (2018) 061601. doi:10.1063/1.5006770.
URL https://doi.org/10.1063/1.5006770

[42] I. M. Sivebaek, B. N. J. Persson, The effect of surface nano-corrugation on the squeeze-out of molecular thin hydrocarbon films between curved surfaces with long range elasticity, Nanotechnology 27 (44) (2016) 445401. doi:10.1088/0957-4484/27/44/445401.
URL https://doi.org/10.1088/0957-4484/27/44/445401

[43] R. Capozza, A. Vanossi, A. Benassi, E. Tosatti, Squeezout phenomena and boundary layer formation of a model ionic liquid under confinement and charging, The Journal of Chemical Physics 142 (6) (2015) 064707. doi:10.1063/1.4907747.
URL https://doi.org/10.1063/1.4907747

[44] R. A. Horne, D. S. Johnson, The viscosity of water under pressure, The Journal of Physical Chemistry 70 (7) (1966) 2182–2190. doi:10.1021/j100879a018.
URL https://doi.org/10.1021/j100879a018

[45] J. W. P. Schmelzer, E. D. Zanotto, V. M. Fokin, Pressure dependence of viscosity, The Journal of Chemical Physics 122 (7) (2005) 074511. doi:10.1063/1.1851510.
URL https://doi.org/10.1063/1.1851510

[46] F. Schmid, Self-consistent-field theories for complex fluids, Journal of Physics: Condensed Matter 10 (37) (1998) 8105–8138. doi:10.1088/0953-8984/10/37/002.
URL https://doi.org/10.1088/0953-8984/10/37/002

[47] P. J. Carreau, Rheological equations from molecular network theories, Transactions of the Society of Rheology 16 (1) (1972) 99–127. arXiv:

https://doi.org/10.1122/1.549276, doi:10.1122/1.549276.
URL https://doi.org/10.1122/1.549276

Supporting Material

S1. Applied force-field parameters

Table S1: Applied force-field parameters (from Refs. [26, 27, 28, 29]). The bond stretching, bending, and torsion terms relate to all 'CH_3', 'CH_2', or 'CH' united-atom groups and their combinations.

non-bonded interactions [12-6 LJ]		
type	ϵ (kcal/mol)	σ (Å)
CH_3	0.2264	3.93
CH_2	0.0933	3.93
CH	0.0794	3.81
Fe	9.5180	2.321

bond streching $[K_r(r-r_0)^2/2]$	
K_r (kcal/mol-Å^2)	r_0 (Å)
536.18	1.54

bending $[K_\theta(\theta-\theta_0)^2/2]$	
K_θ (kcal/mol-rad^2)	θ_0 (deg.)
124.134	114.0

torsion $[K_\phi(1+d\cos(n\phi))]$		
K_ϕ (kcal/mol)	d	n
1.499	1	3

S2. Density & compressibility

Modeling of density (ρ) and compressibility (κ) was conducted based on a pure bulk liquid system (as shown in Fig. S1) with periodic boundary conditions applied in all three dimensions. The cubic cell contains a total number of 200 molecules, resulting in an average volume of 183.2 nm^3 at ambient conditions. In the calculation of density, the temperature (300 K) and pressure (0.1 MPa) were maintained using isothermal-isobaric (NPT) ensemble; while, in the calculation of compressibility, molecules were relaxed at two fixed cell volumes (i.e. $V_1 =$ 183.1 nm^3 and $V_2 = 175.0$ nm^3) where cannonical (NVT) ensemble was adopted. κ was thereby calculated as $\kappa = -\frac{1}{V_1}\frac{\Delta V}{\Delta P}$. For each case, the relaxation time was at least 50 ns. The MD predictions alongside experimental references are shown in Table S2.

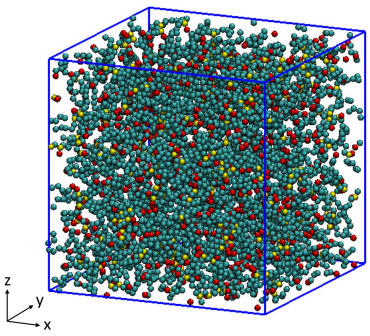

Figure S1: A representative MD cell of bulk 1-decenc trimer (unless specified, the simulation set-up is similar to that in the main text).

Table S2: density (ρ) and compressibility (κ)

	MD	Exp.
ρ (g/cm^3)	0.783	0.783 [37]
κ (1/GPa)	1.12	0.83 [38]

S3. Shear viscosity

Couette flow non-equilibrium molecular dynamics (NEMD) simulations were carried out based on a sandwich-like model shown in Fig. S2(a), where a liquid film (containing 225 1-decene trimer molecules in total) was confined by two parallel iron slabs. The in-plane dimensions of each slab are 5.7×5.1 nm^2, with a confined film thickness (h) of approximately 5.7 nm at ambient pressure. A constant normal load (P_n) of 0.2 GPa was applied on the top slab throughout the simulation; while, displacement of the bottom slab in z-direction was restricted. Periodic boundary conditions were applied in x- and y-direction. The slabs slid in opposite directions along x each at a constant value of $v/2$. In order to ensure stick boundary condition, the solid-liquid interaction was artificially increased. The system pre-slid for at least 10 ns to approaching a steady state, and thereafter data was collected within the next 20 ns.

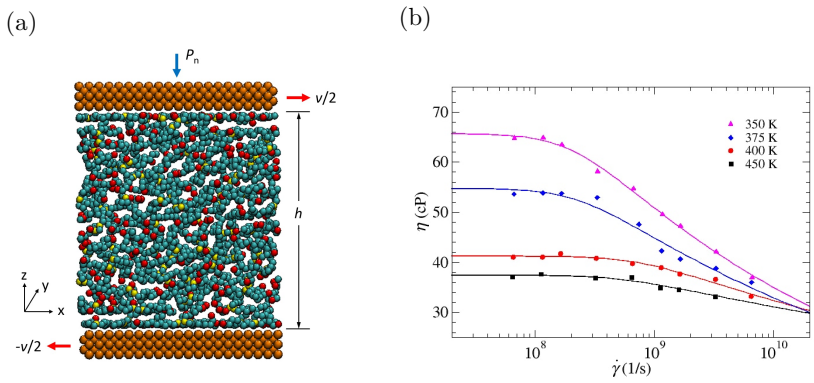

Figure S2: (a) A representative shear model used in the non-equilibrium MD simulations, in which a 1-decene trimer film was confined by two iron slabs. (b) Rate-dependent shear viscosity as a function of temperature (solid curves represent fitting to the *Carreau* equation).

Shear viscosity (η) was calculated based on

$$\frac{F_x}{A} = \eta \cdot \frac{\partial v_x}{\partial z}, \tag{3}$$

where F_x is the x-component (shear) force on the slab, A the contact area, and $\frac{\partial v_x}{\partial z}$ the velocity gradient in z. The simulation was conducted at four

temperatures (i.e. T = 350, 375, 400, and 450 K), each with a shear rate ($\dot{\gamma}$) ranged from 0.55 to 55 GHz. The results are shown in Fig. S2(b), to which the effective shear (Newtonian) viscosity (η_0) at each given temperature was extrapolated through fitting to the *Carreau* [47] equation:

$$\eta = \eta_0[1 + (\frac{\dot{\gamma}}{\dot{\gamma}_0})^2]^{(n-1)/2}, \tag{4}$$

where $\dot{\gamma}_0$ and n are fitting parameters ($\dot{\gamma}_0$ correlates with the inverse of relaxation time, and n varies with temperature and pressure). Detailed fitting information can be found in Table S3. Our calculations agree reasonably well with predictions from previous reports [31, 39].

Table S3: Results of fitting to the MD-predicted shear viscosity using Eq. S2

T (K)	η_0 (cP)	$\dot{\gamma}_0$ (GHz)	n
350	65.67	0.21	0.84
375	54.75	0.24	0.86
400	41.21	0.72	0.91
450	37.41	0.50	0.94